

# Stability of superfluid and supersolid phases of dipolar bosons in optical lattices

Ippei Danshita<sup>1</sup> and Carlos A. R. Sá de Melo<sup>2</sup>

<sup>1</sup>*Department of Physics, Waseda University, Shinjuku-ku, Tokyo 169-8555, Japan*

<sup>2</sup>*School of Physics, Georgia Institute of Technology, Atlanta, Georgia 30332, USA*

(Dated: November 2, 2018)

We perform a stability analysis of superfluid (SF) and supersolid (SS) phases of polarized dipolar bosons in two-dimensional optical lattices at high filling factors and zero temperature, and obtain the phase boundaries between SF, checkerboard SS (CSS), striped SS (SSS), and collapse. We show that the phase diagram can be explored through the application of an external field and the tuning of its direction with respect to the optical lattice plane. In particular, we find a transition between the CSS and SSS phases.

PACS numbers: 03.75.Hh, 03.75.Lm, 05.30.Jp

Since the realization of the superfluid-Mott insulator transition of ultracold Bose gases confined to optical lattices, ultracold atoms have become the playground for the realization of various quantum phases studied in condensed matter physics [1]. The unprecedented control of the lattice depth, dimensionality, geometry, and filling factor has allowed for the exploration of a variety of effects, including the experimental observation of a dipolar condensate of <sup>52</sup>Cr atoms [2, 3, 4] and the production of ultracold heteronuclear molecules [5].

The problem of interacting dipolar bosons is important not only for magnetic dipolar atoms, but also for heteronuclear molecules and Rydberg atoms, which can have potentially large electric dipole moments. Thus far, dipolar superfluids (SF) have been found only for magnetic dipolar atoms in optical traps [2, 3, 4], but there are still several phases that can be pursued experimentally, including dipolar supersolids (SS), which are characterized by the simultaneous existence of crystalline and SF orders. The possibility of SS phases first emerged in the context of solid <sup>4</sup>He [6, 7, 8]. More recently, there have been experimental reports that the theoretically predicted [8] non-classical rotational inertia was found [9] in solid <sup>4</sup>He. Although the existence of a SS still remains a controversial issue in the condensed matter literature [10], its existence may be easier to verify in the context of Bose gases in optical lattices.

In this manuscript, we analyze SF and SS phases of ultracold dipolar Bose gases loaded into two-dimensional (2D) optical lattices, and focus on the region of high filling factors. We show that using an external field the sign and magnitude of dipole interactions can be controlled leading to a variety of different phases. The phases described include SF, striped SS (SSS), checkerboard SS (CSS), and collapse, for which we analyze experimentally relevant quantities such as the excitation spectra.

Our work on ultracold dipolar bosons distinguishes itself from recent work on this topic in several ways. First, our discussion is analytical in contrast to numerical work based on the Gutzwiller projection techniques [11, 12, 13] or quantum Monte Carlo (QMC) methods [14, 15, 16].

Second, while some work [12, 17] was confined to purely repulsive dipolar interactions, we allow for the competition between attractive and repulsive dipolar interactions by changing the direction of an external field with respect to the 2D lattice plane. Third, we explore the phase diagram for a wider range of interactions than previously investigated [11, 12, 13, 17] and find that the quantum phase of the system can be switched between CSS and SSS as the direction of the dipole is changed. The transition between these SS phases is remarkable in the sense that it is a structural phase transition between two types of SS, where the symmetry of the crystalline order changes. Lastly, we go beyond mean-field descriptions by including fluctuation effects and performing a stability analysis.

To study bosons with dipole-dipole interactions in 2D optical lattices, we use the dipolar-Bose-Hubbard model

$$H = -J \sum_{\langle jl \rangle} (b_j^\dagger b_l + \text{h.c.}) + \frac{U}{2} \sum_j n_j (n_j - 1) + \sum_{j < l} V_{jl} n_j n_l, \quad (1)$$

where  $b_j^\dagger$  is the boson creation operator at site  $j$ ,  $n_j = b_j^\dagger b_j$ , and  $J$  is the hopping.  $\langle jl \rangle$  represents nearest-neighbor (NN) pairs of lattice sites. The onsite interaction  $U = U_s + U_d$  consists of the contributions from both the s-wave scattering  $U_s = 4\pi\hbar^2 a_s/m \int d\mathbf{r} |w(\mathbf{r})|^4$  and the onsite dipole-dipole interaction  $U_d = (2\pi)^{3/2} \int d\mathbf{k} \tilde{n}^2(\mathbf{k}) \tilde{V}_d(\mathbf{k})$  [12, 18], where  $a_s$  is the s-wave scattering length,  $w(\mathbf{r})$  is the Wannier function with respect to the underlying lattice potential, and  $\tilde{n}(\mathbf{k})$  and  $\tilde{V}_d(\mathbf{k})$  are the Fourier transform of the density  $|w(\mathbf{r})|^2$  and the dipole-dipole potential. The long-range part of the dipole-dipole interaction is well-approximated as  $V_{jl} = D^2(1 - 3\cos^2\theta_{jl})|\mathbf{r}_j - \mathbf{r}_l|^{-3}$  where  $D$  is the dipole moment and  $\theta_{jl}$  is the angle between the dipole direction and  $\mathbf{r}_j - \mathbf{r}_l$ . Here,  $\mathbf{r}_j = (j_x a, j_y a)$  is a lattice vector, where  $j_x$  and  $j_y$  are integers and  $a$  is the lattice spacing. A schematic picture of the system is shown in Fig. 1.

Since we are interested only in SF and SS phases, we restrict ourselves to Bose-condensed solutions of Eq. (1). Minimizing the quantum action  $S = i\hbar \sum_j b_j^\dagger \partial_t b_j - H$

with respect to the saddle-point field  $\tilde{\Psi}_j(t)$  obtained from the transformation  $b_j(t) \rightarrow \Psi_j(t) = \tilde{\Psi}_j(t) + \delta\Psi_j(t)$ , and neglecting the fluctuations  $\delta\Psi_j(t)$  lead to the time-dependent Gross-Pitaevskii (GP) equation  $i\hbar\partial_t\tilde{\Psi}_j = -J\sum_{\langle l \rangle}\tilde{\Psi}_l + (U|\tilde{\Psi}_j|^2 + \sum_{l\neq j}V_{jl}|\tilde{\Psi}_l|^2)\tilde{\Psi}_j$ . The description above is justified when the healing length  $\xi = \hbar/(m^*c)$  is larger than the interatomic distance  $l = a/\sqrt{\nu}$  [19], where  $c$  is the sound velocity,  $m^*$  is the effective mass, and  $\nu$  is the filling factor. This condition is satisfied when  $J \gg \max(U, |V_{i,j}|)$ . In addition, as discussed later, the emergence of SS phases requires  $J < \nu U$ , which can be satisfied when  $\nu \gg 1$ . Thus, our approach is valid for large hopping and large filling factor. Notice that we are not investigating incompressible solid phases, such as Mott-insulators and density wave solids, because they can not be described within this GP approximation.

Writing  $\tilde{\Psi}_j(t) = \Phi_j e^{-i\mu t/\hbar}$  requires the static part of the condensate  $\Phi_j$  to satisfy

$$-J\sum_{\langle l \rangle}\Phi_l + (U|\Phi_j|^2 + \sum_{l\neq j}V_{jl}|\Phi_l|^2)\Phi_j = \mu\Phi_j, \quad (2)$$

where  $\mu$  is the chemical potential. The normalization condition is  $M^{-1}\sum_j|\Phi_j|^2 = \nu$ , where  $M$  is the total number of sites; and the energy of the condensate is

$$E = -J\sum_{\langle j,l \rangle}(\Phi_j^*\Phi_l + \text{c.c.}) + \frac{U}{2}\sum_j|\Phi_j|^4 + \sum_{j<l}V_{jl}|\Phi_j|^2|\Phi_l|^2. \quad (3)$$

A standard procedure to obtain phase diagrams is the comparison of energies for various phases as done in mean-field studies based on the Gutzwiller projection technique [11, 12, 13]. It is also important to study the stability of each phase in order to construct the correct phase diagram. For this purpose, we perform a stability analysis by taking into account fluctuations  $\delta\Psi_j = e^{-i\mu t/\hbar}(u_j e^{-i\epsilon t/\hbar} - v_j^* e^{i\epsilon^* t/\hbar})$  beyond the saddle-

point  $\tilde{\Psi}_j$ , which lead to the eigenvalue equations

$$-J\sum_{\langle l \rangle}u_l + \left(2U|\Phi_j|^2 + \sum_{l\neq j}V_{j,l}|\Phi_l|^2 - \mu\right)u_j + \Phi_j\sum_{l\neq j}V_{j,l}\Phi_l^*u_l - U\Phi_j^2v_j - \Phi_j\sum_{l\neq j}V_{j,l}\Phi_lv_l = \epsilon u_j, \quad (4)$$

$$-J\sum_{\langle l \rangle}v_l + \left(2U|\Phi_j|^2 + \sum_{l\neq j}V_{j,l}|\Phi_l|^2 - \mu\right)v_j + \Phi_j^*\sum_{l\neq j}V_{j,l}\Phi_lv_l - U(\Phi_j^*)^2u_j - \Phi_j^*\sum_{l\neq j}V_{j,l}\Phi_l^*u_l = -\epsilon v_j. \quad (5)$$

Here,  $\epsilon$  is the energy and  $(u_j, v_j)$  is the amplitude of the collective mode of the condensate. The appearance of collective modes with complex frequencies signals exponential growth of fluctuations in time, and thus the existence of dynamical instabilities (DI).

Since the dipolar interaction decays over distance, the ratios between the NN interactions  $V_x = (1 - 3\sin^2\alpha\cos^2\phi)D^2/a^3$ ,  $V_y = (1 - 3\sin^2\alpha\sin^2\phi)D^2/a^3$  (along the  $x$  and  $y$  directions) and the onsite interaction  $U$  dictates the basic physics. Here,  $\alpha$  and  $\phi$  are the elevation and azimuthal angles of the direction of the polarization with respect to the 2D lattice plane as shown in Fig. 1(b). These ratios are experimentally controllable, e.g., by changing the  $s$ -wave scattering length via a Feshbach resonance, as demonstrated with  $^{52}\text{Cr}$  atoms [4]. Moreover, the ratio  $\gamma = V_y/V_x$  is also controllable by changing the polarization direction through the application of an external field. For instance, when  $\phi = \pi/2$  and  $\alpha$  varies, the relevant ratio becomes  $\gamma = 1 - 3\sin^2\alpha$ .

To gain analytical insight, we consider first onsite and NN interactions. In this case, there are four possible pure condensate phases. When the absolute values of  $V_x$  and  $V_y$  are much smaller than  $U$ , the system is in a SF phase. When the NN interactions are almost isotropic and strongly repulsive, diagonal crystalline order develops and a CSS phase emerges. When the NN interaction is strongly anisotropic, e.g.  $V_x = -V_y$ , a SSS phase is favored. Schematic pictures of these phases are shown in Figs. 2(I)-(IV). The phase boundaries of SF, CSS, and SSS can be determined by solving Eq. (2) and obtaining the ground state energy given in Eq. (3). In addition, strongly attractive NN interactions result in the collapse of the condensate, which is characterized by a DI occurring in the long-wavelength phonon mode. In Fig. 2, the solid and dotted lines indicate the phase boundaries in the  $(V_x/U, V_y/U)$  plane for  $J/(\nu U) = 0.1$ .

Let us first identify the SF region. In the SF phase, the condensate wave function,  $\Phi_j = \sqrt{\nu}$ , is uniform and the chemical potential is  $\mu_{\text{SF}} = -4J + \nu(U + 2V_x + 2V_y)$ . From Eq. (3), we obtain the energy  $E_{\text{SF}}/M = -4J\nu + \nu^2(U + 2V_x + V_y)$ , and from Eqs. (4) and (5) we obtain the excitation spectrum  $\epsilon_{\text{SF}}(\mathbf{q}) = \sqrt{\tilde{\epsilon}(\mathbf{q})[\tilde{\epsilon}(\mathbf{q}) + 2\nu(U + 2V(\mathbf{q}))]}$ , where  $\mathbf{q}$  is the quasimomentum of the collective mode,

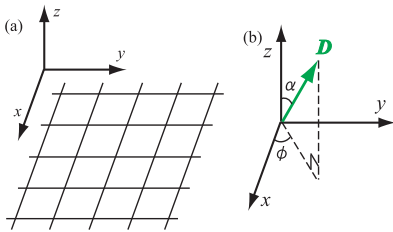


FIG. 1: (color online) (a) Schematic picture of a 2D lattice system, where a square represents a site. (b) The dipole vector is shown in the spherical polar coordinates.

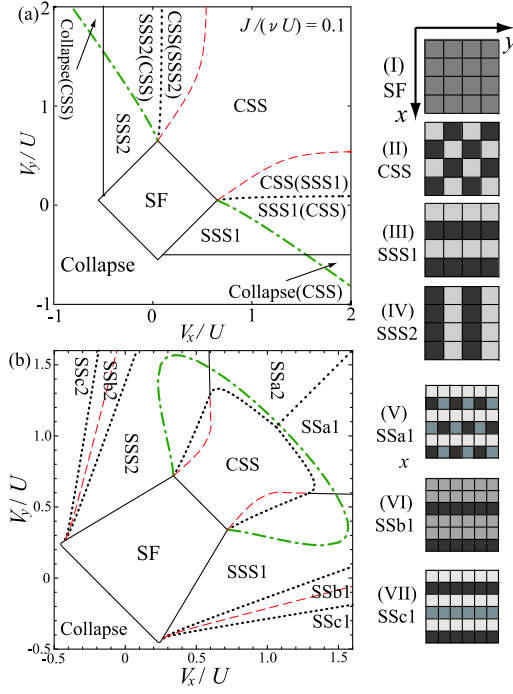


FIG. 2: (color online) Left: Phase diagrams in the  $(V_x/U, V_y/U)$  plane for  $J/(\nu U) = 0.1$ . While only the NN interactions are considered in (a), the full dipolar interactions are included in (b). The solid (dotted) lines represent phase boundaries for continuous (discontinuous) transitions. The dashed-dotted green lines and the dashed red lines separate the stable and unstable regions of the CSS state and those of the SSS. Right: Schematic pictures of SF (I), CSS (II), SSS1 (III), SSS2 (IV), SSa1 (V), SSB1 (VI), and SSc1 (VII).

$$\tilde{\epsilon}(\mathbf{q}) = 4J(\sin^2(q_x a/2) + \sin^2(q_y a/2)), \text{ and } V(\mathbf{q}) = V_x \cos(q_x a) + V_y \cos(q_y a).$$

Since  $\epsilon_{\text{SF}}(\mathbf{q}) = c_{\text{SF}} \hbar q$  for  $qa \ll 1$ , where  $c_{\text{SF}} = \sqrt{2\nu(U + 2V_x + 2V_y)}Ja/\hbar$  is the sound velocity for the SF phase, long-wavelength phonons cause a DI when  $U + 2V_x + 2V_y < 0$  for any non-zero value of  $J$ . The sound velocity  $c$  is directly related to the compressibility  $\kappa$  via  $\kappa^{-1} = m^* c^2$ , which clearly shows that the compressibility becomes negative at this DI leading to the collapse of the condensate [20]. On the other hand, since  $\epsilon_{\text{SF}}(\mathbf{Q}_0) = \sqrt{8J + 2\nu(U - 2V_x - 2V_y)}$ , where  $\mathbf{Q}_0 \equiv (\pi/a, \pi/a)$ , the collective modes in the vicinity of  $\mathbf{Q}_0$  cause a DI when  $2V_x + 2V_y - U - 4J/\nu > 0$ , signaling a transition to the CSS phase [17], where the mode with  $\mathbf{q} = \mathbf{Q}_0$  is amplified and its interference with the condensate in the zero momentum state creates the checkerboard density wave order. Similarly, we find that the collective modes in the vicinity of  $\mathbf{q} = \mathbf{Q}_1 \equiv (\pi/a, 0)$  or  $\mathbf{Q}_2 \equiv (0, \pi/a)$  cause a DI and signal transitions to the SSS phases, when  $2V_x - 2V_y - U - 2J/\nu > 0$  or  $2V_y - 2V_x - U - 2J/\nu > 0$ , respectively. Thus, the SF phase corresponds to the square region surrounded by the lines  $2V_x + 2V_y + U = 0$ ,  $2V_x + 2V_y - U - 4J/\nu = 0$ ,  $2V_x - 2V_y - U - 2J/\nu = 0$

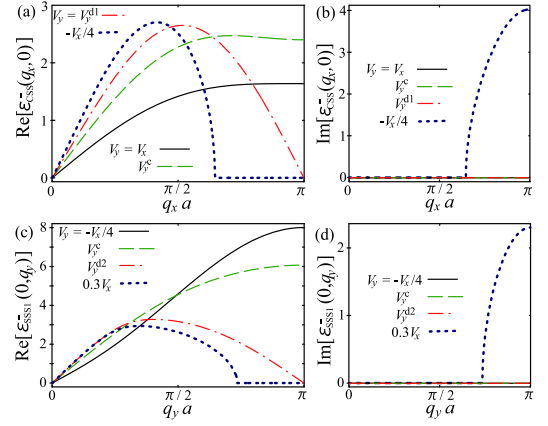


FIG. 3: (color online) Excitation spectra  $\epsilon_{\text{CSS}}^-(q_x, q_y = 0)$  and  $\epsilon_{\text{SSS1}}^-(q_x = 0, q_y)$  for  $J/(\nu U) = 0.1$ , and  $V_x = U$ . (a) The real part and (b) the imaginary parts of  $\epsilon_{\text{CSS}}^-(q_x, q_y = 0)$ . (c) The real part and (d) the imaginary parts of  $\epsilon_{\text{SSS1}}^-(q_x = 0, q_y)$ .

and  $2V_y - 2V_x - U - 2J/\nu = 0$  as shown in Fig. 2(a).

Since the phase diagram is symmetric with respect to the line  $V_x = V_y$ , we focus on the region  $V_x > V_y$  henceforth. The condensate wave functions for the CSS and SSS1 states are  $\Phi_j^{\text{CSS}} = \sqrt{\nu_{c_0}} + \sqrt{\nu_c} e^{i\mathbf{Q}_0 \cdot \mathbf{r}_j}$  and  $\Phi_j^{\text{SSS1}} = \sqrt{\nu_{s_0}} + \sqrt{\nu_s} e^{i\mathbf{Q}_1 \cdot \mathbf{r}_j}$ . Here,  $\nu_c$  ( $\nu_s$ ) is the density of atoms condensed in the state with quasimomentum  $\mathbf{Q}_0$  ( $\mathbf{Q}_1$ ), corresponding to the order parameter of CSS (SSS1). These states are regarded as SS phases in the sense that each of them possesses off-diagonal long-range order through the condensate, and diagonal long-range order via a density wave. From Eq. (2), for the CSS phase we obtain  $\mu_{\text{CSS}} = 2\nu U$ ,  $\nu_{c_0} = \nu - \nu_c$ , and  $\nu_c = \nu/2 - 2J/(2V_x + 2V_y - U)$ . Similarly for SSS1, we obtain  $\mu_{\text{SSS1}} = -2J + 2\nu(U + 2V_y)$ ,  $\nu_{s_0} = \nu - \nu_s$ , and  $\nu_s = \nu/2 - J/(2V_x - 2V_y - U)$ . Since  $\nu_c$  ( $\nu_s$ ) vanishes at the phase boundary between SF and CSS (SSS1), the phase transitions are continuous according to Landau's classification (or second-order according to Ehrenfest's).

From Eq. (3), the energies of the condensate for the CSS and the SSS1 are expressed as  $E_{\text{CSS}}/M = -8J^2/(2V_x + 2V_y - U) + \nu^2 U$ , and  $E_{\text{SSS1}}/M = -2J\nu - 2J^2/(2V_x - 2V_y - U) + \nu^2(2V_y + U)$ . The condition,  $E_{\text{CSS}} = E_{\text{SSS1}}$ , determines the phase boundary between CSS and SSS1 as shown in Fig. 2(a). Both  $\nu_c$  in CSS and  $\nu_s$  in SSS1 are finite at the phase boundary. This fact indicates that the phase transition between CSS and SSS1 is discontinuous (first-order). A discontinuous phase transition is characterized by hysteresis, such that the critical point  $V_y^{d1}$  of the transition from CSS to SSS1 disagrees with the critical point  $V_y^{d2}$  of transition from SSS1 to CSS due to the presence of more than one meta-stable state. To determine  $V_y^{d1}$  and  $V_y^{d2}$ , we calculate the excitation spectra  $\epsilon_{\text{CSS}}^\pm(\mathbf{q})$  and  $\epsilon_{\text{SSS1}}^\pm(\mathbf{q})$  for CSS and SSS1, where the plus (minus) sign corresponds to a gapful (gapless) mode at low momenta.

In Figs. 3(a) and (b), we show  $\varepsilon_{\text{CSS}}^-(q_x, q_y = 0)$  for varying  $V_y$ , but fixed  $V_x = U$ . As  $V_y$  decreases, a roton-like minimum is formed at  $\mathbf{q} = \mathbf{Q}_1$  and reaches zero at  $V_y = V_y^{\text{d}_1}$ . As  $V_y$  is decreased further, the imaginary part of  $\varepsilon_{\text{CSS}}^-(\mathbf{Q}_1)$  grows, thus revealing the transition to the SSS1 phase. The condition  $\varepsilon_{\text{CSS}}^-(\mathbf{Q}_1) = 0$  then gives  $V_y^{\text{d}_1}$  as shown by the dashed-dotted green line in Fig. 2(a). In Figs. 3(c) and (d), we show  $\varepsilon_{\text{SSS1}}^-(q_x = 0, q_y)$  for varying  $V_y$ , but fixed  $V_x = U$ . The condition  $\varepsilon_{\text{SSS1}}^-(\mathbf{Q}_2) = 0$  gives  $V_y^{\text{d}_2}$  as shown by the dashed red line in Fig. 2(a).

To complete our analysis of the phase diagram, we locate now the boundary between phases SSS1 and collapsed. When  $qa \ll 1$ ,

$$\varepsilon_{\text{SSS1}}^-(\mathbf{q}) \simeq \sqrt{2V_y + U} \left( \frac{8J^2(q_x a)^2}{2V_x - 2V_y - U} + 4\nu J(q_y a)^2 \right)^{1/2}, \quad (6)$$

and the DI leads to the collapse when  $2V_y + U < 0$  (see Fig. 2(a)).

Next we numerically calculate the energy and perform linear stability analyses for the full dipolar interactions. We choose a specific case of  $\phi = 0$  or  $\pi/2$ , where the dipolar interactions can be written as  $V_{jl} = (i_x^2 V_x + i_y^2 V_y) / (i_x^2 + i_y^2)^{5/2}$ .  $i_x$  and  $i_y$  are integers that satisfy  $\mathbf{r}_j - \mathbf{r}_l = (i_x a, i_y a)$ . In this case, we obtain the phase diagram in the  $(V_x/U, V_y/U)$ -plane for  $J/(\nu U) = 0.1$  as shown in Fig. 2(b) [21]. As well as in the phase diagram with only the NN interactions, there remain the CSS and SSS regions, which we have confirmed to be stable. CSS shares phase boundaries with SSS and the transition between these two phases is discontinuous (first-order). However, unlike the case with only the NN interactions, there are additional SS phases with different density wave orders, such as SSa, SSb, and SSb (see (V)-(VII) of Fig. 2). While SSb has two-sublattice density modulation as well as CSS and SSS do, SSa and SSb have three-sublattice modulation. There can be other SS phases with more than three-sublattice modulation, which shares boundary with SSa and SSb, but here we do not determine the location of these phases because we are mainly interested in the SF, CSS, and SSS phases.

In phenomenological classical models involving dipolar interactions for 2D continuum systems [22, 23, 24] it has been conjectured that superstructures or micro-emulsion phases exist between two stable phases in a region of the temperature versus density phase diagram where phase separation overrides an otherwise expected first order phase transition. A necessary condition for the emergence of such micro-emulsions at zero temperature is the negative compressibility leading to phase separation. For a first order transition between CSS and SSS described within our model and approach, we do not find a negative compressibility, namely the pre-condition for phase separation, in the transition region. In contrast, recent QMC simulations by Pollet *et al.* have shown pre-

liminary evidence of micro-emulsion phases in systems of hardcore dipolar bosons in a 2D triangular lattice [25]. However, QMC simulations of larger system sizes are necessary to make a conclusive statement about the presence of the micro-emulsion phases.

In conclusion, we have studied stability of quantum phases of dipolar bosons in two-dimensional optical lattices. We have shown that mean-field theories alone fail to describe correctly the phase boundaries, and that a stability analysis is absolutely necessary. In addition to superfluid and collapsed phases, we have shown that striped and checkerboard supersolids can exist, and compete with each other due to the anisotropy of dipolar interactions as controlled by an external field.

We thank D. Yamamoto, L. Pollet and R. Scalleter for useful discussions, and the JQI for their hospitality. I. D. is supported by a Grant-in-Aid from JSPS, and C. SdM thanks NSF (DMR-0709584) and ARO (W911NF-09-1-0220) for support.

- 
- [1] I. Bloch, Nat. Phys. **1**, 23 (2005).
  - [2] A. Griesmaier *et al.*, Phys. Rev. Lett. **94**, 160401 (2005);
  - [3] J. Stuhler *et al.*, Phys. Rev. Lett. **95**, 150406 (2005).
  - [4] T. Lahaye *et al.*, Nature (London) **448**, 672 (2007).
  - [5] C. Ospelkaus *et al.*, Phys. Rev. Lett. **97**, 120402 (2006).
  - [6] A. F. Andreev and I. M. Lifshitz, Sov. Phys. JETP **29**, 1107 (1969).
  - [7] C. V. Chester, Phys. Rev. A **2**, 256 (1970).
  - [8] A. J. Leggett, Phys. Rev. Lett. **25**, 1543 (1970).
  - [9] E. Kim and M. H. W. Chan, Nature (London) **427**, 225 (2004); Science **305**, 1941 (2004).
  - [10] S. Sasaki *et al.*, Science **313**, 1098 (2006).
  - [11] K. Góral *et al.*, Phys. Rev. Lett. **88**, 170406 (2002).
  - [12] C. Menotti *et al.*, Phys. Rev. Lett. **98**, 235301 (2007).
  - [13] S. Yi *et al.*, Phys. Rev. Lett. **98**, 260405 (2007).
  - [14] A. van Otterlo *et al.*, Phys. Rev. Lett. **72**, 3598 (1994); G. G. Batrouni *et al.*, *ibid.* **74**, 2527 (1995).
  - [15] P. Sengupta *et al.*, Phys. Rev. Lett. **94**, 207202 (2005).
  - [16] G. G. Batrouni and R. T. Scalettar, Phys. Rev. Lett. **84**, 1599 (2000); F. Hébert *et al.*, Phys. Rev. B **65**, 014513 (2001).
  - [17] D. L. Kovrizhin *et al.*, Europhys. Lett. **72**, 162 (2005).
  - [18] C. Menotti *et al.*, AIP Conf. Proc. **970**, 332 (2008).
  - [19] L. P. Pitaevskii and S. Stringari, *Bose-Einstein Condensation* (Oxford Science Publications, Oxford, 2003).
  - [20] D. Rychtarik *et al.*, Phys. Rev. Lett. **92**, 173003 (2004).
  - [21] In practical calculations, we include all  $V_{jl}$  that satisfies  $|\mathbf{r}_j - \mathbf{r}_l| \leq 300a$ , where full convergence is achieved.
  - [22] S. Kivelson and S. A. Trugman, Phys. Rev. B **33**, 3629 (1986).
  - [23] K.-O. Ng and D. Vanderbilt, Phys. Rev. B **52**, 2177 (1995).
  - [24] B. Spivak and S. A. Kivelson, Phys. Rev. B **70**, 155114 (2004).
  - [25] L. Pollet *et al.*, arXiv:0906.2126.